

Mechanisms of Nanoglass Ultrastability

Denis Danilov,[†] Horst Hahn,^{†,‡} Herbert Gleiter,^{†,§} and Wolfgang Wenzel^{*,†}

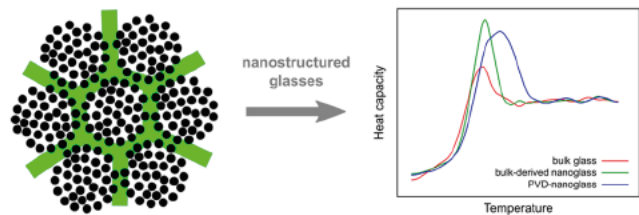
[†]Institute of Nanotechnology, Karlsruhe Institute of Technology, 76344 Eggenstein Leopoldshafen, Germany

[‡]KIT TUD Joint Research Laboratory Nanomaterials, TU Darmstadt, 64287 Darmstadt, Germany

[§]Institute of Nanoscience, Nanjing University of Science and Technology, 210094 Nanjing, China

Supporting Information

ABSTRACT: The origin of the astonishing properties of recently discovered ultrastable nanoglasses is presently not well understood. Nanoglasses appear to exhibit density variations not common in bulk glasses and differ significantly in thermal, magnetic, biocompatible, and mechanic properties from the bulk materials of the same composition. Here, we investigate a generic model system that permits modeling of both the physical vapor deposition process (PVD) of the nanoparticles and their consolidation into a nanoglass. We performed molecular dynamics simulations to investigate the PVD process generating nanometer sized noncrystalline clusters and the formation of the PVD nanoglass when these nanoclusters are consolidated. In agreement with the experiments, we find that the resulting PVD nanoglass consists of two structural components: noncrystalline nanometer sized cores and interfacial regions that are formed during the consolidation process. The interfacial regions were found to have an atomic structure and an internal energy that differ from the structure and internal energy of the corresponding melt quenched glass. The resulting material represents a noncrystalline state that differs from a bulk glass with the same chemical composition and a glass obtained from nanoparticles derived from the bulk glass.



KEYWORDS: nanoglasses, physical vapor deposition, ultrastable glasses, molecular dynamics simulations

Today's technologies are based to a large extent on crystalline materials such as metal, semiconductors or ceramics, in large part because it is possible to control their properties (*e.g.*, mechanical strength, electric conductivity, optical properties, *etc.*) by either modifying their chemical microstructure (*e.g.*, by introducing different phases, by varying their chemical compositions, *etc.*) or by the controlled introduction of lattice defects (such as intercrystalline interfaces, dislocations, *etc.*) or by both.¹ In most glassy materials, comparable structural modifications are not possible. At present, glasses are most frequently produced by cooling the melt, and hence, they essentially inherit its atomic structure. Nanoglasses are a new class of noncrystalline solids which are synthesized by consolidating nanoparticles obtained by physical vapor deposition or sputtering into a bulk material^{1–5} to generate a new kind of noncrystalline solids that permit the controlled modification of the defect and/or the chemical microstructures of noncrystalline solids by methods that are comparable to the methods used today for crystalline materials.^{6–8} Figure 1 illustrates schematically similarities and differences between nanocrystalline and nanoglass materials. A melt (Figure 1a) solidifies into a single crystal, which can be processed into crystalline nanoparticles (Figure 1b) that have the same internal structure as the crystal. These nanoparticles can be consolidated (Figure 1c) into a material with a high density of defects in the form of incoherent interfaces (Figure 1d). In analogy, nanometer sized glassy particles obtained from

a PVD process (Figure 1e) are consolidated (Figure 1f) into a bulk material.^{6–8} In contrast to crystalline materials, it is presently unclear how the characteristics of the resulting noncrystalline material (Figure 1g), called nanoglass, differ from the corresponding bulk glass. In the crystalline material, the difference in the lattice orientation of different grains prevents their consolidation into a homogeneous single crystal, but there is no corresponding long range order in glasses. Nevertheless, studies of the atomic and the electronic structure of a variety of metallic nanoglasses (for reviews, we refer to refs 1–4) support a structural model suggesting that nanoglasses consist of two kinds of noncrystalline regions: glassy regions resulting from the consolidated nanometer sized glassy clusters (Figure 1f) and interfacial regions between these consolidated glassy clusters (green regions in Figure 1g). The heterogeneous granular structure of nanoglasses is accompanied by a number of remarkable material properties, such as thermal ultra stability,⁹ enhanced magnetic properties,¹⁰ improved biocompatibility,¹¹ and an enhanced thermal stability of the amorphous interfaces between the amorphous regions in the nanoglasses.^{12,13}

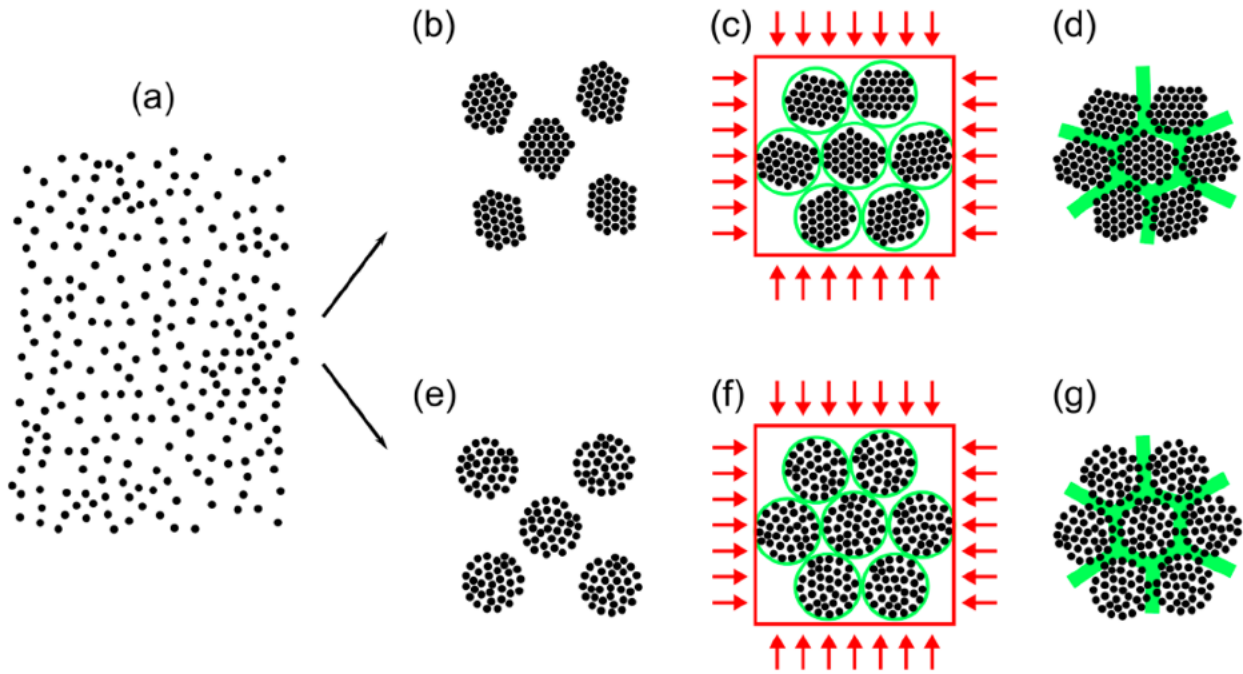


Figure 1. Schematic analogy between the defect and the chemical microstructures of nanocrystalline materials and nanoglasses: (a) melt, (b) single crystal nanoparticles, (c) consolidation process, and (d) the microstructure of nanocrystalline materials is stabilized by the crystal orientation of the different grains; (e) glassy nanoparticle, (f) consolidation process, and (g) the mechanism for the stabilization of distinct phases in nanoglasses is unknown.

There is presently no conceptual framework or model to explain these unusual properties of nanoglasses. Simulations of model systems which permit detailed characterization of each step of the process may offer insights into the mechanism that are presently difficult to obtain experimentally. However, molecular dynamics simulations of nanoglasses with realistic interatomic potentials struggle with the long time scales and have, to date, not been able to reproduce the experimental results reported above, in particular with regard to the existence of a second, stable glassy phase in the interfacial regions between the grains.^{14,15} It has been a fundamental assumption of previous simulation studies that samples derived from bulk glasses have been used as a source of material for the glassy grains. In this study, we go beyond this assumption and investigate a model that incorporates the preparation process of the nanoparticles and their consolidation into the bulk materials. As will be shown below, both the properties of the amorphous nanoparticles from which the PVD nanoglass is formed and the interfacial regions differ from those of bulk glasses of the same composition. Our model is motivated by recent studies of ultrastable bulk glasses,¹⁶ which suggest that enhanced surface mobility in the physical vapor deposition (PVD) process may change the properties of the nanoparticle cores in comparison to bulk glasses with the same composition. When these cores are consolidated into a bulk material, the large surface to volume ratio of the nanoparticles results in fundamental changes in the properties of the consolidated material.

RESULTS AND DISCUSSION

In the following, we investigate a Kob–Andersen model system,¹⁷ with a computational protocol that mimics the preparation processes of PVD nanoglasses: (i) condensation of nanoparticles from a gas phase and (ii) consolidation of the nanoparticles into the nanoglass in order to study structure and

thermal stability of the nanoglass. To simulate the PVD condensation of nanoparticles from the gas phase, a molecular dynamics deposition protocol is applied in which new atoms of the Kob–Andersen AB mixture with a ratio of 80/20 are continuously added to the simulation box at random positions to represent the gas phase (for details see [Methods](#)). The atoms subsequently attach at the free surface of a spherical nanoparticle (formed at early stage of the deposition process) until the resulting nanoparticle has achieved a size of $\approx 30\,000$ atoms. This size corresponds to cluster radius ≈ 20 in dimensionless units or roughly 4.4 nm when converted to a comparable physical system. For comparison, we also prepared with the same composition the atomic structure of a bulk glass consisting of 10 000 atoms. [Figure 2](#) shows the average potential energy per atom of the nanoparticles as a function of the deposition temperature and potential energy per atom of bulk glass as a function of the final temperature of the cooling process. Due to a strong segregation of the A atoms at or near the cluster surface, the chemical composition of the nanoparticles in the central region is roughly $A_{77}B_{23}$ and hence differs from the $A_{80}B_{20}$ composition of the gas phase. In addition, [Figure 2](#) also displays the data for a bulk glass prepared with a composition $A_{77}B_{23}$. This composition corresponds roughly to the composition of the interior of the nanoparticles at temperatures above the glass transition temperature. [Figure 2](#) shows that the nanoparticles have lower potential energy per atom in comparison to the corresponding bulk glass.

Typical radial profiles of composition and potential energy per atom in the nanoparticles are shown in [Figure 3](#). We observe a monotonic increase of the potential energy from the center of the nanoparticle to the outside. The central region of the cluster is characterized by a nearly constant potential energy which is below the potential energy of the corresponding bulk glass (*cf.* [Figure 2](#)). In the vicinity of the cluster surface, a steep

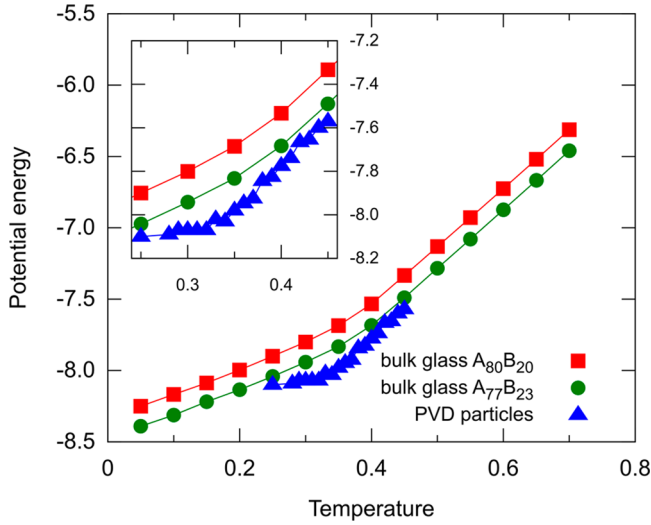


Figure 2. Potential energy for bulk glass at different final temperatures of the cooling process in comparison to PVD nanoparticles at different deposition temperatures.

increase of the potential energy is observed. This increase is accompanied by a compositional change. In fact, the fraction $c_A(r)$ of A atoms approaches 100% at the free surface. We use the onset of the increase of the potential energy to define a radius R_c that divides the nanoparticle into a core region with $r < R_c$ and a surface region with $r > R_c$. As may be seen from Figure 3, the increase of $c_A(r)$ consists of two slowly varying regions with a crossover in the first half of the surface region ($r > R_c$) followed by a saturation in the outermost shell.

In the subsequent step of the simulation, the nanoparticles (prepared at the deposition temperature $T = 0.32$) were consolidated at a pressure of $p = 1.5$ into a nanoglass, which corresponds to the consolidation procedure used in the experimental studies to prepare PVD nanoglasses. The simulation box before and after consolidation is shown in Figure 4. For visualization of the simulation results, the atoms in the core and the surface regions of the nanoparticles are labeled in red (core atoms in Figure 4) and blue or green (atoms in the surface regions, Figure 4). As may be seen from Figure 4, no significant diffusion occurs between the core and surface regions during or after the consolidation process.

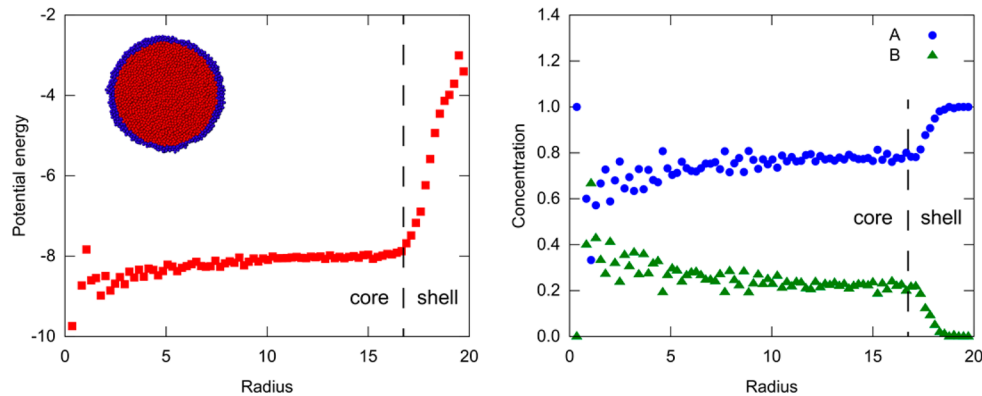


Figure 3. Radial profiles of potential energy and composition in a nanoparticle prepared by vapor deposition (in the right panel: blue circles/green triangles correspond to the concentration of A/B atoms, respectively). Inset in the left panel shows a cross section of the nanoparticle with red atoms representing the core and blue atoms representing the shell.

The density and the volume fraction of the nanoparticle cores and of the interfacial regions formed during consolidation were computed by means of a Voronoi tessellation. Figure 4 shows the density within the cores and within the interfaces during the consolidation process. In fact, as far as the evolution of the densities in the core and the interfacial regions during consolidation are concerned, three stages (labeled s_1 , s_2 , s_3 in Figure 4) may be distinguished. In the first stage, s_1 , when the pressure increases linearly from $p = 0$ to $p = 1.5$, the outer shells of the nanoparticles start to form amorphous interfaces. The average density of these interfaces rapidly increases, while the density of the cores increases far less. In the second stage, s_2 , when the system is equilibrated at a pressure of $p = 1.5$, the density of cores remains unchanged, and the density of the interfaces increases slightly by atomic rearrangements that close the small holes that have remained after the stage s_1 . However, at all times, the density of the interfacial regions remained lower than that the density of the cores. In stage s_3 , the pressure is relaxed linearly to $p = 0$ and the densities of cores and the interfaces decrease uniformly by approximately the same amount. Finally (after the relaxation of the stage s_3), the system was equilibrated for 10 times the simulation time of the entire consolidation process. The difference in the density between the amorphous grains and the amorphous interfaces remains stable throughout this phase of the simulation.

To investigate the thermal stability of the bulk glass in comparison to the PVD nanoglass, both structures were incrementally heated mimicking the experimental differential scanning calorimetry process. The resulting enthalpy data were fitted to an analytical expression (see Supporting Information) to obtain the heat capacity shown in Figure 5. When the temperature was increased, a phase transition was observed, as indicated by a peak in the heat capacity (Figure 5). Table 1 shows the onset temperature T_o , the peak temperature T_p , the width σ_p of the temperature range in which the phase transition takes place, and the enthalpy ΔH , defined as the integrated specific heat over the peak region, of the phase transition. Clearly, the onset temperatures and the temperatures of the peaks of the heat capacity of the bulk glass and of the PVD nanoglass differ. In fact, the bulk glass is found to be less stable than the PVD nanoglass. At the same time, the highest value of ΔH , accompanied by the largest width σ_p of the transition temperature, of the PVD nanoglass is almost two times wider than the one of the bulk glass. To unequivocally demonstrate

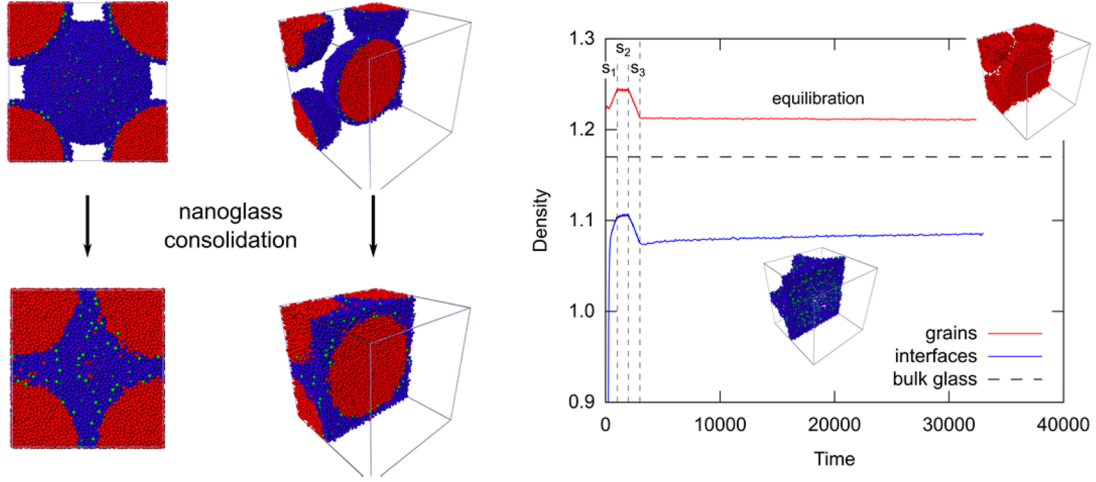


Figure 4. Consolidation of nanoparticles into a nanoglass and evolution of the density of core (grains) and shell (interfaces) groups of atoms during consolidation and during the subsequent equilibration. The red atoms show both A and B atoms in cores. The blue color indicates the A atoms within the shells, and green color corresponds to the B atoms within the shells. The right panel shows the density of the central region and interface region in red/blue, respectively. The density of the bulk glass is given by the dashed line for reference.

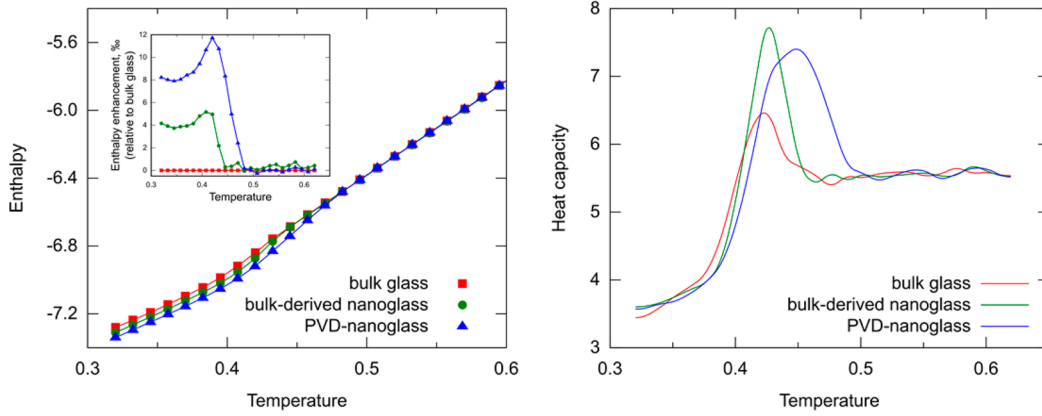


Figure 5. Left: enthalpy of the glass cooled from the melt (red), the bulk derived nanoglass (green), and the PVD nanoglass (blue). The inset shows the deviation of the ratio of the enthalpy of the bulk derived nanoglass and the PVD nanoglass relative to the bulk glass (positive deviations indicate a lower energy). Right: heat capacity of bulk glass, PVD nanoglass, and bulk derived nanoglass as a function of temperature.

Table 1. Transition Temperature T_p , Heat of Transition ΔH (See Definition in Text), Width σ_p of the Temperature Range, and the Onset Temperature T_r

	T_p	ΔH	σ_p	T_r
bulk glass	0.418	0.066	0.017	0.343
bulk-derived nanoglass	0.425	0.103	0.015	0.361
PVD-nanoglass	0.442	0.194	0.027	0.371

that these features arise as a result of the PVD process, we have prepared nanoparticles of the same size and composition by cutting the bulk glass into fragments, which were then subjected to the same consolidation process as the PVD nanoparticles. Figure S2 shows the evolution of the densities during the consolidation of amorphous particles derived from the bulk. The resulting material, called bulk derived nanoglass, features a variation in density of 0.86% that is more than 10 times smaller than in the case of PVD nanoparticles where the variation is 10.9%. The existence of the small density variation in the bulk derived nanoglass can be attributed to a limited reorganization of atoms at the surface of the nanoparticles derived from the bulk glass. Along with the small density

variation, the reorganization has an effect of decreasing the enthalpy of the bulk derived nanoglass compared to the bulk glass. We have investigated the bulk derived nanoglass only to demonstrate that the enthalpy of the PVD nanoglass cannot be reached when bulk derived glass fragments undergo the same process that we used to simulate the consolidation of the PVD glass particles to the bulk material (see Figure 5). To our knowledge, there is no experimental protocol to break the bulk glass into nanoparticles while preserving its structure, and therefore, the bulk derived nanoglass has no experimental counterpart. Table 1 shows that the consolidation at the high pressure leads to an increase in the heat of transition ΔH , as defined above, but does not lead to the thermal ultrastability as the transition temperature T_p only slightly differs from the value of the bulk glass. These findings demonstrate that both the interior of the cores and the interfacial regions in PVD nanoglasses differ from their bulk glass counterparts.

Using molecular dynamics simulations, we have investigated (1) the mechanism by which nanoparticles are formed during a PVD process and (2) the processes that result in the formation of a PVD nanoglass when these nanoparticles are consolidated.

In agreement with the experimental observations, our results indicate that the resulting PVD nanoglass materials comprise two structural components, cores resulting from PVD process (high density region) and interfacial low density regions separating the cores. We stress that the label high and low density refer to the relative density of the two regions in the nanoglass. In our study, the density of the high density regions in the nanoglass is higher than that of a bulk glass with the same overall composition as the nanoglass, but it is possible that this order of densities is different in experimental realizations of the system. However, both in our model and experiment, the low density phase has a lower density than bulk glass to the same overall composition. This low density phase delocalizes during consolidation to fill all the available volume in the interstitial regions (see movie in the [Supporting Information](#)). The results of the simulations reported here thus agree with the results of recent studies on nanometer sized glassy clusters as well as with studies on several metallic nanoglasses. Mapping of the chemical composition of $\text{Sc}_{75}\text{Fe}_{25}$ nanoparticles by means of STEM indicated (see Figure S4 in supplementary information to ref 12) the surface regions were found to be enriched in Sc. The reduced density and the width of the interfacial regions of nanoglasses have been studied by SAXS and HRTEM, as well as PAS for ScFe and for AuCuSiAlPd nanoglasses.^{9,13} In fact, the observed reduced interfacial density¹² and interfacial widths agree well with our model.

In our model for the PVD nanoglass, both the nanoparticle cores and interfacial regions differ from their bulk equivalents: [Figures 4 and 5](#) indicate that the PVD growth process of nanometer sized clusters results in a noncrystalline structure which differs from the structure obtained by quenching the bulk melt. It is presently not known whether this is the case for the experimental realizations of nanoglasses. In the model, this effect results from the deposition procedure, which is not accessible by quenching the melt. The packing of the nanoparticle cores is analogous to recent PVD experiments, which create glassy materials of organic molecules with extraordinary thermodynamic and kinetic stability. The elastic moduli of these so called ultrastable organic glasses exceed those of ordinary glass by up to 19%.¹⁸ Matrix assisted pulsed laser evaporation has been used to form ultrastable, nano structured glassy polymer films which, relative to the ordinary glass, are 40% less dense, have a 40 K higher glass transition temperature, and exhibit a 2 orders of magnitude enhancement in kinetic stability at high temperatures.^{19,20} These exceptional properties are not limited to organic materials. Recently, also ultrastable metallic glasses with an enhanced thermal stability, a higher glass transition temperature, and an enhanced elastic modulus were created by vapor deposition.²¹ Numerical simulations¹⁶ using binary model system¹⁷ confirm the hypothesis that the ultrastability of these systems results from the enhanced surface mobility of the constituents during deposition. The same seems to apply to the different thermal stability of nanoglasses in comparison to melt quenched glasses with the same chemical composition. DSC studies of AuCuSiAlPd nanoglasses^{5,9} revealed an enhanced thermal stability of the nanoglass. For example, the crystallization temperature of the nanoglass was about 25 K higher.

These observations suggest a mechanism for the stabilization of the glass–glass interfaces in [Figure 1g](#). The interfacial regions are formed during the consolidation process and remain stable because the PVD process leads to ultrastable particles with a variation of the composition. The segregation of the A atoms to

the surface of nanoparticles (see [Figure 3](#)) is a universal consequence of the difference of interaction energies between the different components of the glass, but this does not result in complete demixing. In a finite nanoparticle, the overall free energy of the particle will be lower, when strongly interacting particles aggregate preferentially in the core (many neighbors).

This effect is a result of the deposition process creating the particles and has no equivalent when quenching the melt into a bulk glass. This variation in stoichiometry is the equivalent to variation of long range lattice orientation in adjacent grains that stabilizes grain boundaries in crystalline materials ([Figure 1d](#)). It also explains why the stable interfacial regions observed in this investigation differ from those of simulations starting from bulk glasses: In the latter, only the short range order of the glass is perturbed through the introduction of grain boundaries, which comprise a much smaller fraction of the material than observed in nanoglasses. In nanoglasses, the surface material delocalizes to fill the entire free volume in the consolidation process, in a framework provided by the nanoparticle cores (see movie in [Supporting Information](#)). As a result, the nanoglass consists of two regions, the high density region comprising the former nanoparticle cores or some fraction thereof and the novel low density region filling the interfaces. The reduced density at the interfaces does not automatically lead to an overall reduced density of the nanoglass, which will depend on the consolidation condition and final volume fractions of the low density and high density regions.

Our results explain why prior molecular dynamics simulations could not observe the density variation characteristic of PVD nanoglasses observed in experiment. In simulations of Cu–Zr glasses, an internal interface generated by joining two planar surfaces derived from bulk glasses, the interstitial material in the interface allows for shear band formation at lower stress compared to a bulk glass sample,¹⁵ in contrast to experimental observations. In the context of our model, these systems correspond to bulk glass derived nanoglasses that have different properties than PVD nanoglasses. In these systems, the glass–glass interfaces act as structural heterogeneities, which promote shear band formation and prevent strain localization.²²

CONCLUSION

In summary, the present model offers a mechanism for the existence of two stable phases with different densities in nanoglasses consolidated from nanoparticles obtained from vapor deposition. The simulations agree with experimental observations that indicate that the unusual properties of PVD nanoglasses obtained by consolidating nanoparticles¹ seem to result from the properties of the core as well as from the properties of interfacial regions. According to the results obtained ([Figures 4 and 5](#)), the density and internal energy of the interfacial regions differ from the ones of glasses (with the identical chemical composition) prepared by quenching the melt. This difference may be rationalized by the boundary conditions of the two regions: the presence of an interface to the vacuum of the isolated nanoparticles results in a different composition near the surface. Similarly, the cores of the nanoparticles impose boundary conditions on the atoms situated in the interfacial regions between these nanoparticles, which differ from the boundary conditions in a bulk glass. Our simulations suggest that the high surface to volume ratio of the nanoscale environment provided by the nanoparticle cores stabilizes a free energy minimum in the interfacial regions that

cannot be achieved when a bulk glass with the same chemical composition is produced by quenching the melt. To demonstrate that the interfaces of a nanoglass present a unique thermodynamic state, we have prepared body centered, face centered and simple cubic arrangements of the nanoparticles with different volume fractions of interfacial regions. As indicated by Table 2, the potential energy and density of the

Table 2. Properties of the Interfacial Regions of Nanoglasses in Comparison to the Bulk Glass of the Same Composition

	interfaces in "sc" PVD-nanoglass	interfaces in "bcc" PVD-nanoglass	interfaces in "fcc" PVD-nanoglass	A ₈₈ B ₁₂ bulk glass
potential energy per atom	7.52	7.49	7.50	7.38
density	1.09	1.08	1.09	1.07

interfacial material is the same for all three arrangements, indicating that there is a proximity effect resulting in a stable state of the interfacial material with a unique chemical composition. In this study, we have focused on the enhanced thermal stability of the PVD nanoglass and the computational results agree with the experimental data on nanoglass ultrastability. In our model, the enthalpy of the nanoglass is lower than the enthalpy of the bulk glass despite the added free volume that arises through the condensation process. This is in contrast to the expected behavior of the uniform bulk glass, where more free volume will lead to higher energy.

While the present model thus agrees in several important aspects with experimental observations, it has limits in the description of the electronic structure which may differ in the different phases, leading to magnetism and other effects that cannot be treated in a purely classical model. Experimental studies on several metallic nanoglasses indicated that the core regions and the interfacial regions of nanoglasses differ not only as far as their atomic structure is concerned, but also in terms of their electronic structure. In the interfacial regions, a reduced s electron density, a different hyperfine field, differently sized ferromagnetic clusters, an enhanced Curie temperature, and an enhanced plasticity have been observed.^{10,23–25} As differences in the electronic structure between the core and the interfacial regions modify the interatomic interactions, modeling of these effects is beyond the approximations used in the studies reported in this paper.

METHODS

Molecular Dynamics Simulations. Molecular dynamics simulations are performed using LAMMPS²⁶ software package available at <http://lammps.sandia.gov>. Lennard-Jones parameters for Kob-Andersen mixture are $\epsilon_{AA} = 1$, $\sigma_{AA} = 1$, $\epsilon_{AB} = 1.5$, $\sigma_{AB} = 0.8$, $\epsilon_{BB} = 0.5$, $\sigma_{BB} = 0.88$. The masses of the atoms are $m_A = 1$ and $m_B = 1$. The Boltzmann constant is $k_B = 1$. The length is measured in σ_A and the energy is measured in ϵ_A . The dimensionless time unit is equal to

$$t_0 = m_A \sigma_A^2 / \epsilon_A \approx 1. \text{ We use cut off distance 2.5 for the Lennard}$$

Jones potential and the time step $\Delta t = 0.005$. The temperature and pressure are controlled by a Nose Hoover thermostat with damping parameter $100\Delta t$ and barostat with damping parameter $1000\Delta t$.

Bulk Glass. To prepare bulk glass, we simulate a rapid cooling in NPT ensemble. After an initial equilibration at a high temperature $T_1 = 0.9$ for 10^3 time units, *i.e.*, 2×10^5 MD steps, the system is cooled down to final temperature T_2 with cooling rate 10^{-4} followed by final equilibration at T_2 for 10^3 time units.

Vapor Deposition. The vapor deposition protocol is applied to grow a film (periodic boundary conditions are applied in x and y directions and repulsive walls in z direction) or a nanoparticle (repulsive walls in all direction). A number of new atoms is added in regions which are separated from the growing film or the growing nanoparticle by at least 1.2 and the width of the regions is 1.3. The positions of the repulsive walls are adjusted accordingly and the size of the simulation box grows during the deposition. For each deposition step, we perform 2×10^6 MD steps (10^4 time units) at constant volume and temperature T_0 . After the required total number of atoms is deposited by the sequence of many deposition steps, we run NVT equilibration at temperature T_0 for 10^4 time units, *i.e.*, 2×10^6 MD steps.

Nanoglass Consolidation. Consolidation of nanoparticles into the nanoglass is simulated in NPT ensemble at temperature T_0 and includes several steps at different values of the pressure. First step consists of 2×10^5 MD steps (10^3 time units) at pressure linearly increasing from $p = 0$ to $p = 1.5$. Second step is the equilibration at $p = 1.5$ for 2×10^5 MD steps (10^3 time units). On the last step, we relax the pressure linearly from $p = 1.5$ to $p = 0$ for 2×10^5 MD steps (10^3 time units). After the consolidation is done, we equilibrate the system for several 10^4 time units, *i.e.*, several 10^6 MD steps at $T = T_0$ and $p = 0$.

Thermal Stability. The thermal stability of the structures is analyzed by a sequence of NPT runs at the pressure $p = 0$ and increasing temperature. First, equilibration run at temperature T_0 for 100 time units (2×10^4 MD steps) is simulated followed by heating run from T_0 to $T_1 = T_0 + \Delta T$ for 100 time units. Then, we repeat equilibration at T_i and heating to $T_{i+1} + \Delta T$ with $\Delta T = 0.0125$. During the equilibration runs, we collect average value of the enthalpy per atom. The obtained set of points T_i, H_i is fitted to approximate function $H(T)$ and heat capacity C_p is determined as $C_p = \partial H / \partial T$.

Size Estimates. The parameters of the Kob-Andersen model system are dimensionless. To simplify the comparison of the simulations results to the experimental data, the order of magnitude of corresponding physical systems can be obtained with size parameters $\epsilon_{AA} = 0.2$ eV, $\sigma_{AA} = 2.2$ Å, and $m_A = 58.69$ u, which results in a unit time of 0.4 ps. The physical temperature, pressure, and density scales corresponding to the reduced units in the model are then 2321 K, 2.9 GPa, and 8.8 g/cm³, respectively.

ASSOCIATED CONTENT

Supporting Information

The Supporting Information is available free of charge on the ACS Publications website at DOI: 10.1021/acsnano.5b05897.

Additional simulation data (PDF)

Movie (AVI)

AUTHOR INFORMATION

Corresponding Author

*E mail: wolfgang.wenzel@kit.edu.

Notes

The authors declare no competing financial interest.

ACKNOWLEDGMENTS

D.D. acknowledges support from Russian Foundation for Basic Research (RFBR Project No.14 29 10282 ofi m). This work was performed on the computational resource bwUniCluster funded by the Ministry of Science, Research and the Arts Baden Württemberg and the Universities of the State of Baden Württemberg, Germany, within the framework program bwHPC. H.H. and H.G. gratefully acknowledge the financial support by Deutsche Forschungsgemeinschaft under Grant HA 1344/30 1 within the Priority Programme SPP 1594, "Topological Engineering of Ultra Strong Glasses".

REFERENCES

- (1) Gleiter, H.; Schimmel, T.; Hahn, H. Nanostructured Solids – from Nano Glasses to Quantum Transistors. *Nano Today* **2014**, *9*, 17–68.
- (2) Gleiter, H. Our Thoughts Are Ours, Their Ends None of Our Own: Are There Ways to Synthesize Materials Beyond the Limitations of Today? *Acta Mater.* **2008**, *56*, 5875–5893.
- (3) Andrievski, R. A. Metallic Nano/Microglasses: New Approaches in Nanostructured Materials Science. *Phys. Usp.* **2013**, *56*, 261–268.
- (4) Gleiter, H. Nanoglasses: A New Kind of Noncrystalline Materials. *Beilstein J. Nanotechnol.* **2013**, *4*, 517–533.
- (5) Chen, N.; Frank, R.; Asao, N.; Louzguine Luzgin, D. V.; Sharma, P.; Wang, J. Q.; Xie, G. Q.; Ishikawa, Y.; Hatakeyama, N.; Lin, Y. C.; Esashi, M.; Yamamoto, Y.; Inoue, A. Formation and Properties of Au Based Nanograined Metallic Glasses. *Acta Mater.* **2011**, *59*, 6433–6440.
- (6) Jing, J.; Krämer, A.; Birringer, R.; Gleiter, H.; Gonser, U. Modified Atomic Structure in a Pd Fe Si Nanoglass: A Mössbauer Study. *J. Non Cryst. Solids* **1989**, *113*, 167–170.
- (7) Gleiter, H. Nanocrystalline Solids. *J. Appl. Crystallogr.* **1991**, *24*, 79–90.
- (8) Gleiter, H. Are There Ways to Synthesize Materials Beyond the Limits of Today? *Metall. Mater. Trans. A* **2009**, *40*, 1499–1509.
- (9) Wang, J. Q.; Chen, N.; Liu, P.; Wang, Z.; Louzguine Luzgin, D. V.; Chen, M. W.; Perepezko, J. H. The Ultrastable Kinetic Behavior of an Au Based Nanoglass. *Acta Mater.* **2014**, *79*, 30–36.
- (10) Ghafari, M.; Hahn, H.; Gleiter, H.; Sakurai, Y.; Itou, M.; Kamali, S. Evidence of Itinerant Magnetism in a Metallic Nanoglass. *Appl. Phys. Lett.* **2012**, *101*, 243104.
- (11) Chen, N.; Shi, X.; Witte, R.; Nakayama, K. S.; Ohmura, K.; Wu, H.; Takeuchi, A.; Hahn, H.; Esashi, M.; Gleiter, H.; Inoue, A.; Louzguine, D. V. A Novel Ti Based Nanoglass Composite with Submicron–Nanometer Sized Hierarchical Structures to Modulate Osteoblast Behaviors. *J. Mater. Chem. B* **2013**, *1*, 2568–2574.
- (12) Fang, J. X.; Vainio, U.; Puff, W.; Würschum, R.; Wang, X. L.; Wang, D.; Ghafari, M.; Jiang, F.; Sun, J.; Hahn, H.; Gleiter, H. Atomic Structure and Structural Stability of Sc₇₅Fe₂₅ Nanoglasses. *Nano Lett.* **2012**, *12*, 458–463.
- (13) Chen, N.; Louzguine Luzgin, D. V.; Xie, G. Q.; Sharma, P.; Perepezko, J. H.; Esashi, M.; Yavari, A. R.; Inoue, A. Structural Investigation and Mechanical Properties of a Representative of a New Class of Materials: Nanograined Metallic Glasses. *Nanotechnology* **2013**, *24*, 045610.
- (14) Şopu, D.; Albe, K.; Ritter, Y.; Gleiter, H. From Nanoglasses to Bulk Massive Glasses. *Appl. Phys. Lett.* **2009**, *94*, 191911.
- (15) Ritter, Y.; Şopu, D.; Gleiter, H.; Albe, K. Structure, Stability and Mechanical Properties of Internal Interfaces in Cu₆₄Zr₃₆ Nanoglasses Studied by Md Simulations. *Acta Mater.* **2011**, *59*, 6588–6593.
- (16) Singh, S.; Ediger, M. D.; de Pablo, J. J. Ultrastable Glasses from in Silico Vapour Deposition. *Nat. Mater.* **2013**, *12*, 139–144.
- (17) Kob, W.; Andersen, H. C. Testing Mode Coupling Theory for a Supercooled Binary Lennard Jones Mixture I: The Van Hove Correlation Function. *Phys. Rev. E: Stat. Phys., Plasmas, Fluids, Relat. Interdiscip. Top.* **1995**, *51*, 4626–4641.
- (18) Kearns, K. L.; Still, T.; Fytas, G.; Ediger, M. D. High Modulus Organic Glasses Prepared by Physical Vapor Deposition. *Adv. Mater.* **2010**, *22*, 39–42.
- (19) Guo, Y.; Morozov, A.; Schneider, D.; Chung, J. W.; Zhang, C.; Waldmann, M.; Yao, N.; Fytas, G.; Arnold, C. B.; Priestley, R. D. Ultrastable Nanostructured Polymer Glasses. *Nat. Mater.* **2012**, *11*, 337–343.
- (20) Ediger, M. D.; Yu, L. Polymer Glasses: From Gas to Nanoglobular Glass. *Nat. Mater.* **2012**, *11*, 267–268.
- (21) Yu, H. B.; Luo, Y.; Samwer, K. Ultrastable Metallic Glass. *Adv. Mater.* **2013**, *25*, 5904–5908.
- (22) Albe, K.; Ritter, Y.; Şopu, D. Enhancing the Plasticity of Metallic Glasses: Shear Band Formation, Nanocomposites and Nanoglasses Investigated by Molecular Dynamics Simulations. *Mech. Mater.* **2013**, *67*, 94–103.
- (23) Witte, R.; Feng, T.; Fang, J. X.; Fischer, A.; Ghafari, M.; Kruk, R.; Brand, R. A.; Wang, D.; Hahn, H.; Gleiter, H. Evidence for Enhanced Ferromagnetism in an Iron Based Nanoglass. *Appl. Phys. Lett.* **2013**, *103*, 073106.
- (24) Franke, O.; Leisen, D.; Gleiter, H.; Hahn, H. Thermal and Plastic Behavior of Nanoglasses. *J. Mater. Res.* **2014**, *29*, 1210–1216.
- (25) Wang, X. L.; Jiang, F.; Hahn, H.; Li, J.; Gleiter, H.; Sun, J.; Fang, J. X. Plasticity of a Scandium Based Nanoglass. *Ser. Mater.* **2015**, *98*, 40–43.
- (26) Plimpton, S. Fast Parallel Algorithms for Short Range Molecular Dynamics. *J. Comput. Phys.* **1995**, *117*, 1–19.